International Journal of Nanoelectronics and Materials
Volume 16 January 2023 [81-91]

Temperature Effects on the Optical Properties of Bismuth Nanoparticles Prepared by PLAL for Antibacterial Activity

Sally S. Hassan[1], Raad M. S. Al-Haddad[2], and Kadhim A. Hubeatir[1,*]

[1] Department of Laser and Optoelectronics Engineering, University of Technology, Iraq
[2] Department of Physics, College of Science, University of Baghdad, Iraq

Received 13 June 2022, Revised 24 July 2022, Accepted 15 August 2022

ABSTRACT

Bismuth nanoparticles (Bi NPs) constitute a promising technology for combating infectious illnesses and bacterial resistance to antibacterial treatments. Bi NPs were synthesized by Pulsed Laser Ablation in Liquid (PLAL) using a 532 nm second-harmonic generation Nd:YAG laser. Bi NPs samples were prepared in 10, 35, 50, 75, and 90 ˚C water for various laser energies and number of laser pulses. Ultraviolet-visible (UV-Vis) spectra measurements revealed a characteristic plasmonic absorption band indicative of metallic bismuth nano-sized particles. Field emission scanning electron microscopy (FESEM) analysis showed that the water temperature during the ablation process affected the size and morphology of Bi NPs. The average Bi NP size at 60 ˚C was 28 nm, considerably smaller than the 55 nm average observed at 10 ˚C. The antimicrobial properties of Bi NPs against two opportunistic pathogens, E. coli and S. aureus, were assessed. For S. aureus, the inhibition zone of Bi NPs prepared at 60 ˚C was greater than that of samples prepared at 10 ˚C. Further, Bi NPs exhibited lower potency against E. coli than S. aureus in both samples.

Keywords: Pulsed laser ablation in liquid, Nd:YAG laser, Bismuth (Bi) nanoparticles, antibacterial effect, Gram-negative and gram-positive bacteria

1. INTRODUCTION

Antibacterial activity is associated with compounds that kill or slow the growth of bacteria without being toxic to the surrounding tissue [1]. Due to the widespread use and abuse of antibacterial agents, the rise of bacterial resistance to antibacterial treatments has become a prevalent phenomenon, posing a substantial challenge [2]. Nanotechnology, which deals with matter at the nanoscale from 1-100 nm scale [3], provides a solid foundation for modifying the physicochemical characteristics of different materials to develop efficient antimicrobials [4-8]. Microscopic observations revealed that nanoparticles don't penetrate bacterial cells; They adhere to their walls [9]. Thus assessing nano-bio interactions necessitates the adsorption of engineered NP onto bacterial cells. The interaction between synthesized NPs and the cells' surface begins with high adsorption energy. The spontaneity of the process is determined by the total interaction energy between the approaching surfaces [10,11].

Bismuth (Bi) is a semimetal element that is non-toxic for human consumption (lethal intake > 5–20 g/day/kg, for years) [12,13]. The cosmetic and pharmaceutical industries have utilized bismuth compounds for over 250 years [14] and bismuth subsalicylate has been used to treat diarrheal diseases since the 1900s under the brand name Pepto-Bismol. Bismuth compounds have recently been employed in computed tomography imaging and anti-cancer therapies [15]. Exhibiting antibacterial, fungicidal, and antiviral properties, bismuth nanoparticles (Bi NPs) constitute a potential approach to combat infectious illnesses, but additional research is needed to verify their safety for humans. Until it is determined that they are harmless to humans, Bi NPs

* Kadhim.A.Hubeatir@uotechnology.edu.iq

can be used as surface sanitizers in hospitals, geriatric and pediatric clinics, pharmaceutical and food industries, and in general all locations where sources of contamination need to be counteracted [16].

Over decades of research, multiple techniques have been developed to synthesize NPs [17]. Pulsed Laser Ablation in Liquids (PLAL) enables the production of NPs with little or no by-products [18]. A solid substrate submerged in a liquid is irradiated with an ultrashort (10-15–10-9 s) focused laser beam, producing high-temperature and high-density plasma [19]. PLAL has gained popularity because it is a chemically simple and clean synthesis process that can be conducted at standard atmospheric pressure and temperature, and yields excellent product purity. Furthermore, the structures and characteristics of products can be precisely controlled by modifying the experimental variables such as the laser parameters, solvents, surrounding environment, and target material [20-24].

The overall process of NP formation is often characterized by two crucial and interconnected sequential processes in materials synthesis and engineering: nucleation and growth [25]. The first step is nucleation, wherein monomers, such as ions, atoms, or molecules, establish a new thermodynamic structure or configuration at the atomic or molecular level. This process is followed by growth in which monomers become incorporated onto the wall of the nuclei, which may coalesce or aggregate, resulting in a size increase. In many instances, nucleation and growth happen simultaneously and are thus dynamically competitive. The nucleation and growth stages are critical for determining the precise structural characteristics of the material in its final solid form and, as a result, permeate all parts of the industries relying on these materials' specific functionalities [26,27]. Each material nucleates and grows in response to the conditions existing during the synthesis process, and even minute changes in parameters can result in entirely different mechanisms. [28]. One such parameter with a substantial impact is temperature. Interaction temperature on interfacial energy, diffusion and growth rate coefficients, and equilibrium solubility depend on interaction temperature. In turn, these factors affect crystal or grain characteristics at the microstructural level during the phase transition. Temperature is, therefore, an attainable control parameter that may be tuned to enhance product properties and manufacturing methods. Prior studies have demonstrated that the size of NPs decreases as temperature increases [29-32].

Localized Surface Plasmons (LSP) are defined as charge density oscillations restricted to metallic NPs. The excitation of LSPs by an incident electromagnetic field at a specific wavelength induces resonance, which leads to significant light scattering and increased intensity of the localized electromagnetic field [33]. Surface Plasmon Resonance (SPR) in metallic NPs produces a broad spectrum of colors and allows for various optical properties that depend on particle size and shape [34,35].

While the effects of laser parameters on Bi NPs has been investigated in multiple studies, to our knowledge, no research has been conducted on the impact of ablation environment temperature on the structure, morphology, and antibacterial activity of the synthesized Bi NPs. This study attempts to determine whether deliberate engineering of nanomaterials with higher adsorption energy may lead to enhanced antibacterial performance.

2. MATERIALS AND METHODS

2.1. Materials

Bismuth granules (Evek, Germany, purity 99.999%) were pressed without adhesives for five minutes by a 12-ton hydraulic jack to form circular targets with a 1 cm diameter and a 5 mm thickness. The NPs were synthesized using a Q-Switched Nd:YAG Laser Workstation (Marson &

Co., South Africa). A CE-HOTSTR2 Deluxe Lab Hot Plate with a magnetic stirrer (Ayushmaan Scientific Co. & Welchem Trading, India) was used throughout the experimental process to heat and stir the colloidal solution during ablation. The Bi target was placed inside a 25 ml Pyrex glass beaker with an inner diameter of 34 mm and a height of 50 mm. Bi NPs were synthesized in distilled water.

2.2. Experimental Procedure

Metallic Bi NPs were prepared using the PLAL technique as shown in Figure 1. The experimental setup, employed a second-harmonic generation Nd:YAG laser at the 532 nm wavelength operating at a 3 Hz pulse repetition frequency (PRF) with an 8 ns pulse duration. The bismuth targets rested at the bottom of Pyrex glass beakers containing 5 ml of distilled water. A magnetic stirrer, used at a speed of 1600 RPM, provided constant stirring of the colloidal solution during the ablation process to ensure homogeneous fragmentation and optimize nanoparticle formation. The laser beam was focused using a lens of 12 cm focal length. The ablation process was repeated on multiple Bi targets for various values of the laser energy (400, 600, 800, and 1000 mJ), number of laser pulses (300, 400, and 500), and water temperature (10, 35, 50, 75, and 90 ˚C). The optical characteristics of the resulting colloidal Bi solutions were assessed via Ultraviolet-Visible (UV-Vis) spectroscopy immediately after laser ablation, without allowing the NPs to aggregate.

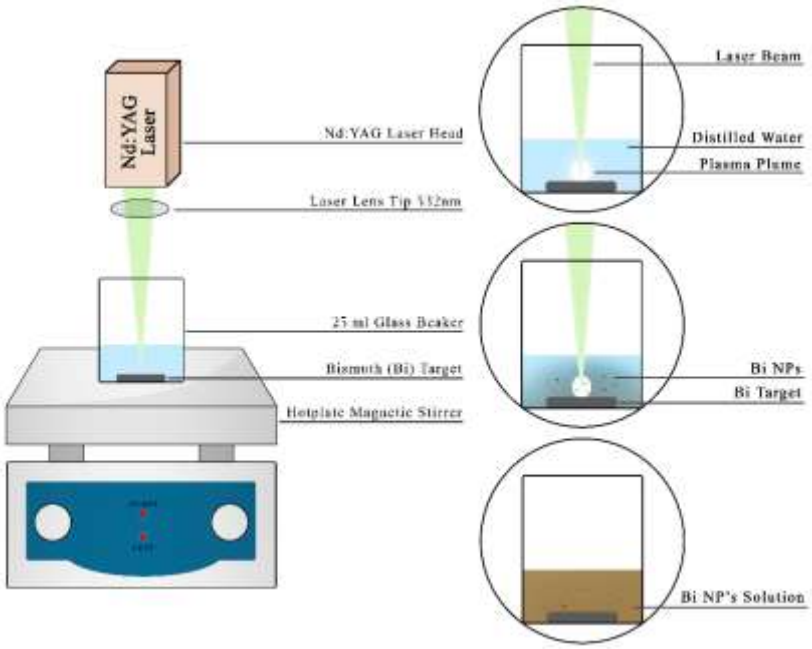

Figure 1. Schematic diagram of the experimental setup used for synthesizing the Bi NPs using PLAL.

2.3. Characterization of Nanoparticles

The optical properties of Bi NPs were assessed using three analytical techniques. UV-Vis absorption spectra were measured using a Metertech SP-8001 UV/Visible Spectrophotometer to characterize optical absorbance. Bi NPs were poured in a quartz cuvette and scanned for wavelengths between 190 nm to 1100 nm using distilled water as the reference, and a scan speed of 500 nm/min. To determine the chemical composition of the Bi NPs, an Oxford Instruments X-Max EDXS System was used to obtain Energy dispersive X-ray spectroscopy (EDXS) measurements. Finally, the structure and morphology of the Bi NPs were investigated via Field-Emission Scanning Electron Microscopy (FESEM) using a High-Resolution FESEM-Zeiss Sigma.

2.4. Assessment of Antibacterial Activity

To assess the possible bactericidal activity of Bi NPs, their effects on gram-negative Escherichia coli (E. coli) and gram-positive Staphylococcus aureus (S. aureus) bacteria were determined. Using an agar well diffusion experiment, the antibacterial activity of the synthesized nanostructures against these two bacterial strains was evaluated. Approximately 20 mL of Muller–Hinton (MH) agar was aseptically placed into sterile Petri dishes. The bacteria were extracted from their stock cultures using a sterile wire loop. After the organisms had been cultured, 6 mm-diameter holes were drilled in the agar plates with a sterile point. Bi NPs solutions with concentrations of 25, 50, 75, and 100% were injected into the drilled wells. The cultivated plates containing the NPs and test organisms were incubated at 37 °C overnight before measuring and recording the average diameter of the inhibition zones. Statistical data analysis was performed using GraphPad prism software. Data are represented as mean ± SD of three experiments and indicate a statistically significant difference with $p < 0.05$.

3. RESULTS AND DISCUSSION

Pulsed laser ablation of the bismuth target in distilled water initially produced dark-brown colloidal solutions. For most samples, the liquid began to turn clear 20–30 minutes after the ablation procedure, quickly transitioning from honey-like to transparent in under 60 minutes (Figure 2); this constitutes a prevalent trend for Bi NPs in prepared samples.

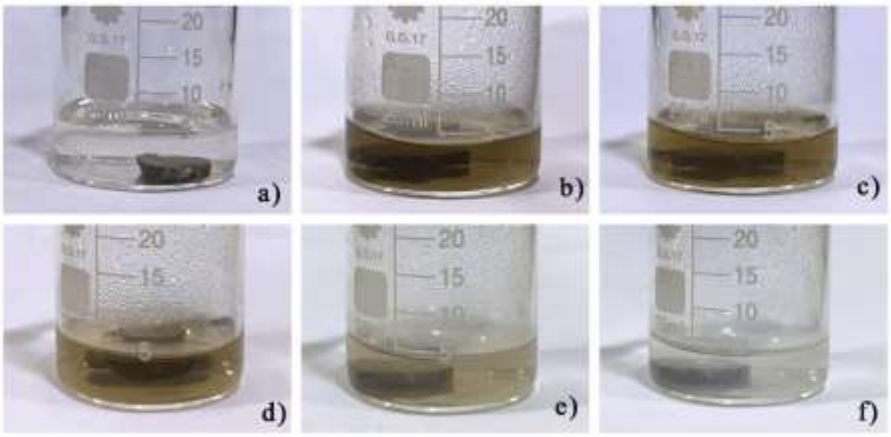

Figure 2. Colloidal solution of Bi NPs in the beaker at 75˚C water temperature a) before PLAL b) immediately after PLAL, after c) 15 minutes, d) 30 minutes, e) 45 minutes, and f) 60 minutes.

3.1. UV-Visible Optical Absorbance Spectra

UV-Vis spectra measurements give are indicative of the shape distribution, size, and scale of generated NPs via analysis of the produced SPR. The absorbance spectra of unspecified concentrations of Bi NPs are shown in Figures (3-5). The absorption peak positions vary with the laser energy, water temperature, and number of pulses. Absorbance consistently peaks under 270 nm, which is representative of previously reported values for Bi NPs. The Bi NPs' SPR absorption peak, which gradually increases as the size of the Bi NPs decreases; this explains the observed absorbance peaks. Our spectra indicates that the shape of the Bi NPs are spheres with a diameter larger than 10 nm but lower than 100 nm, which is consistent with the FESEM data presented in section 3.3.

3.1.1. Effect of Laser Energy

To determine optimal ablation energy, laser energies of 400, 600, 800, and 1000 mJ were used with preparation conditions of 3 Hz and 400 pulses. Results, shown in Figure 3a), indicate that the largest redshift and lowest absorbance intensity occur at 400 mJ. Increasing the laser energy leads to an increase in absorbance intensity without any major blue shift. To determine the optimal laser energy, the absorbance intensity and absorbance peak positions were graphed as a function of laser energy [Figure 3b)]. Two intersections can be seen at 650 mJ and 1000 mJ. Because 650 mJ has the lowest wavelength of the two, it was chosen as the optimal energy to conduct this experiment.

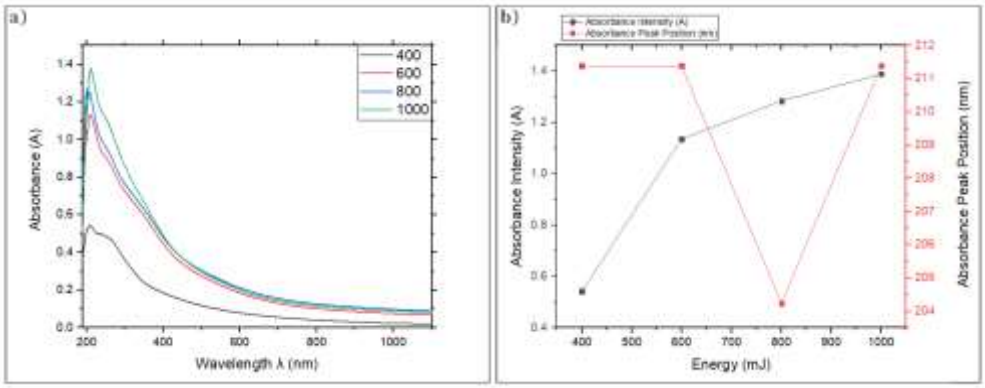

Figure 3. a) UV-Vis spectra showing the SPR absorbance of Bi NPs for laser energies of 400, 600, 800, and 1000 mJ. b) SPR absorbance intensity and absorbance peak position of Bi NPs as functions of laser energy.

3.1.2. Effect of Number of Laser Pulses

Bi NPs samples were produced with 300, 400, and 500 laser pulses. Figure 4a) displays the influence of the number of laser pulses on the absorbance spectra. Figure 4b) represents the absorbance intensity and peak position as a function of the number of pulses. Results indicate that the optimal number of laser pulses among all samples is 410.

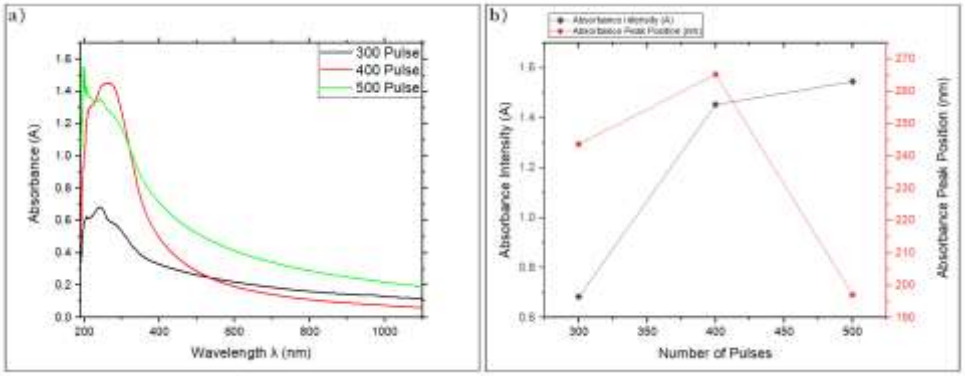

Figure 4. a) UV-Vis spectra showing the SPR absorbance of Bi NPs for 300, 400, and 500 laser pulses. b) SPR absorbance intensity and absorbance peak position of Bi NPs as functions of the number of laser pulses.

3.1.3. Effect of Water Temperature

Samples were synthesized at 650 mJ, 410 laser pulses, and for water temperatures of 10, 35, 50, 75, and 90˚C. The effects of water temperature variations on the SPR absorbance are illustrated in Figure 5. Absorbance intensity varied nonlinearly with water temperature. The optimal water temperature can be inferred from Figure 5b). Intersections can be identified at 40, 60, and 80 ˚C, with the absorbance peak position increasing slightly with temperature. The choice was eventually made to study the effects of a 60˚C water temperature to better understand the effects of the increase in water temperature.

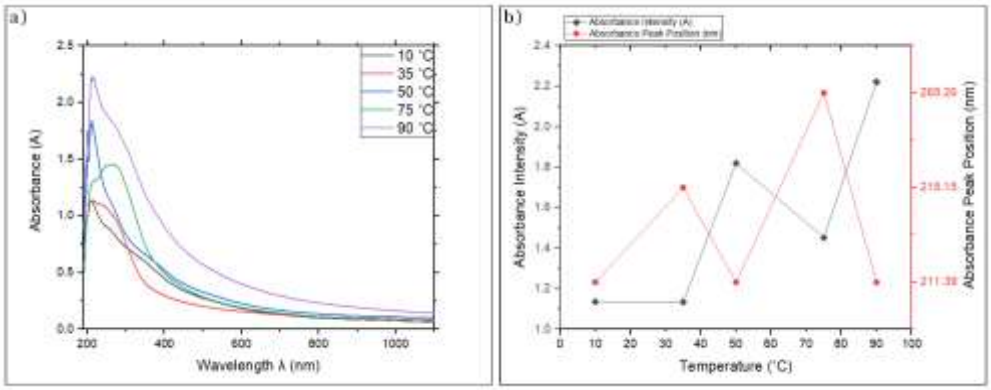

Figure 5. a) UV-Vis spectra showing the SPR absorbance of Bi NPs for water temperatures of 10, 35, 50, 75, and 90 ˚C. b) SPR absorbance intensity and absorbance peak position of Bi NPs as functions of water temperature.

After analysis of the results shown in Figures 3b), 4b), and 5b), the following parameters were chosen as the optimal preparation conditions and used for the EDXS and FESEM analyses: 650 mJ laser energy, 410 laser pulses, and 60 ˚C water temperature. To fully grasp the effects of water temperature on the size distribution and antibacterial activity of Bi NPs, results were compared for 10 ˚C and 60 ˚C water temperature, all other parameters remaining constant.

3.2. EDXS Chemical Analysis

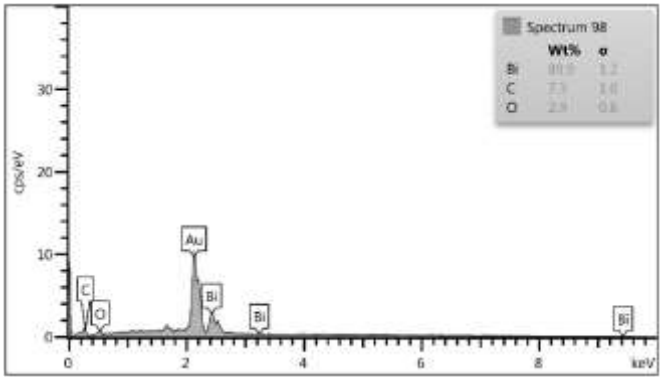

Figure 6. EDXS spectrum of prepared Bi NPs.

The chemical composition of the prepared NPs was investigated via EDXS analysis to identify the elements making up the synthesized Bi NPs. Spectra from isolated particles shown in Figure 6 confirm the presence of bismuth in the NPs. In EDXS analysis, samples are commonly coated with a very conductive metal to render non-conductive materials conductive, and to enhance the signal-to-noise ratio, which results in higher-quality images [36]. For this reason, Figure 6 also

shows prominent gold peaks. In addition, the presented stoichiometry confirms our successful preparation of Bi NPs.

3.3. FESEM imaging of Bi NPs Structure and Morphology

Morphology and size distribution of Bi NPs were characterized via FESEM [Figures 7a) and 8a)]. The size distribution was estimated by manually analyzing the FESEM images, measuring individual particles using ImageJ software [Figures 7b) and 8b)]. The average particle size was estimated at 55 ± 8 nm at 10 ˚C water temperature (Figure 7) and 28 ± 8 nm at 60 ˚C (Figure 8). Results, therefore, indicate that samples synthesized at 10 ˚C produced larger-sized NPs compared to samples prepared at 60 ˚C. Further investigation of Figure 8a) revealed the occurrence of nucleation with the growth of Bi NPs, which exist as nanoclusters, enhancing the adsorption energy of NPs. A higher reaction temperature leads to the formation of smaller NPs and to a narrower size distribution. Conversely, a lower reaction temperature results in larger NPs and a broader size distribution. This can be explained by the higher kinetic energy associated with higher temperature, which increases collisions between initially formed nanoparticles, thus reducing particle size [32]. These findings suggest a more significant effect on bacterial strains for the sample synthesized at 60˚C.

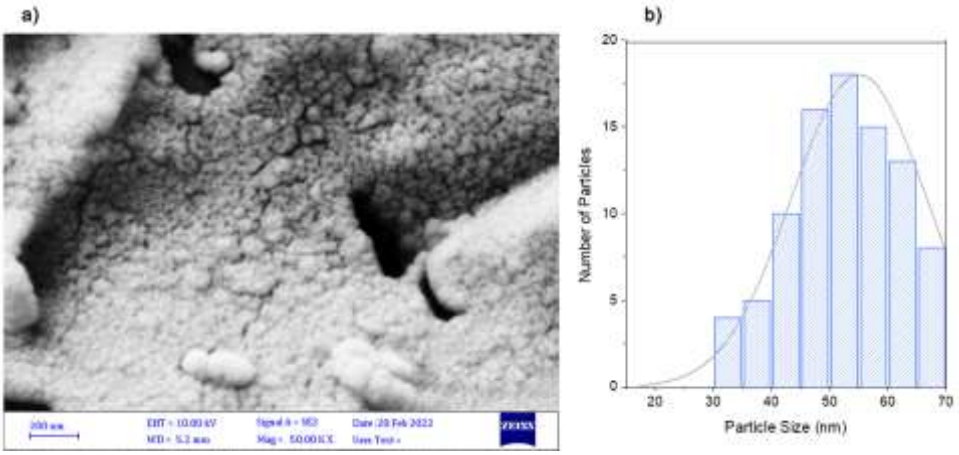

Figure 7. a) FESEM-generated image and b) size distribution of Bi NPs prepared at 10˚C, 650 mJ, 3 Hz PRF, and 410 pulses.

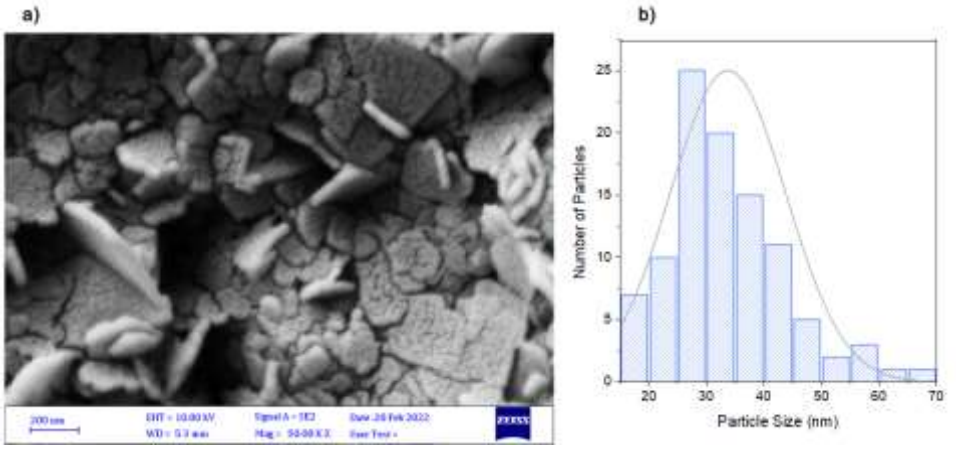

Figure 8. a) FESEM- generated image and b) size distribution of Bi NPs prepared at 60˚C, 650 mJ, 3 Hz PRF, and 410 pulses.

For convenience and to avoid redundancy, we will refer to these samples as A and B before delving into their effects as antibacterial agents. Experimental parameters used to synthesize samples A and B are outlined in Table 1.

Table 1 Values of experimental parameters for Samples A and B

Sample Name	Water Temperature (T)	Laser Energy (E)	Pulse Repetition Frequency (PRF)	Number of Pulses
	(˚C)	(mJ)	(Hz)	
A	10	650	3	410
B	60	650	3	410

3.4. Antibacterial Activity

Figures 9-12 depict the inhibition zone after representative microorganisms' exposure to various concentrations of Samples A and B. For each sample, the impact on both bacterial strains was 4 5 times greater than for the control. Moreover, results indicate that Bi NPs have a significantly stronger effect on gram-positive bacteria than gram-negative bacteria. For *E. coli*, reducing the concentration of Sample A resulted in a linear decrease in the inhibition zone size (Figure 9). For Sample B (Figure 10) the inhibition zone was thinner for 75% concentration than for 50% concentration, increasing in size again for 100% concentration. Sample A outperforms Sample B in terms of antibacterial activity against *E. coli*, although by a small margin. *S. aureus* shows a great susceptibility to Bi NPs (Figures 11 and 12). In contrast to results obtained for *E. coli*, the inhibition zone does not linearly increase with concentration with *S. aureus* bacteria. Results indicate that the water temperature significantly impacts NPs' antibacterial activity, in correlation with our previously stated estimations. These findings concur with the research published by P. Domenico et al. [37], establishing that Gram-negative bacteria were more prone to resist the inhibitory action of bismuth. According to their research, this resistance is related to the competitive relationship between iron and bismuth among Gram-negative bacteria, the concentration and uptake mechanisms of iron playing a key role in bismuth resistance. Their report documents that bismuth-treated bacteria produced outer membrane proteins similar in size to iron-repressible proteins.

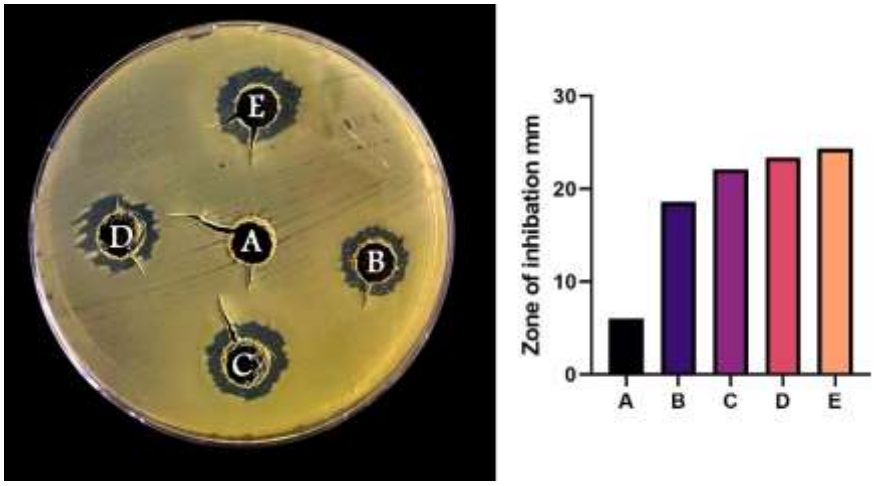

Figure 9. Antibacterial activity of (Sample A) against *E.Coli.* A, control. B, 25%. C, 50%. D, 75%. E, 100%.

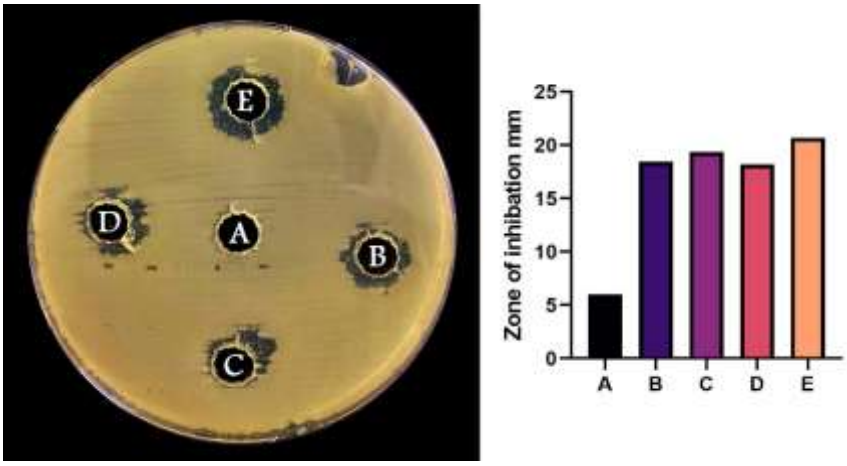

Figure 10. Antibacterial activity of (Sample B) against E.Coli. A, control. B, 25%. C, 50%. D, 75%. E, 100%.

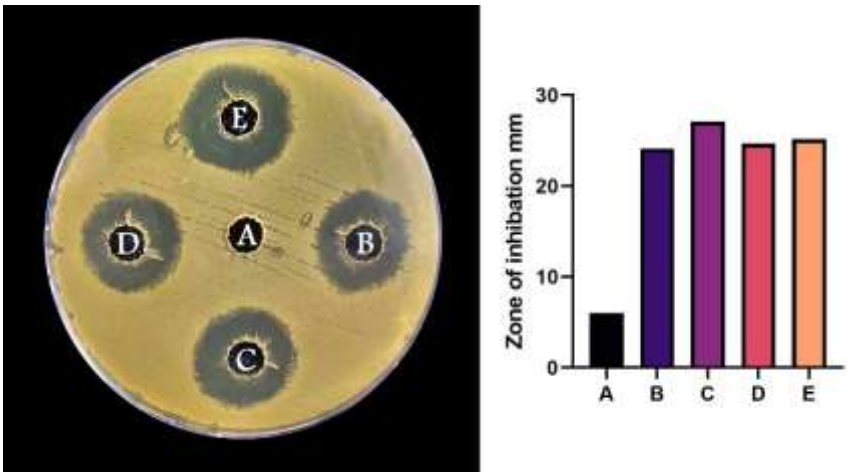

Figure 11. Antibacterial activity of (Sample A) against S. aureus. A, control. B, 25%. C, 50%. D, 75%. E, 100%.

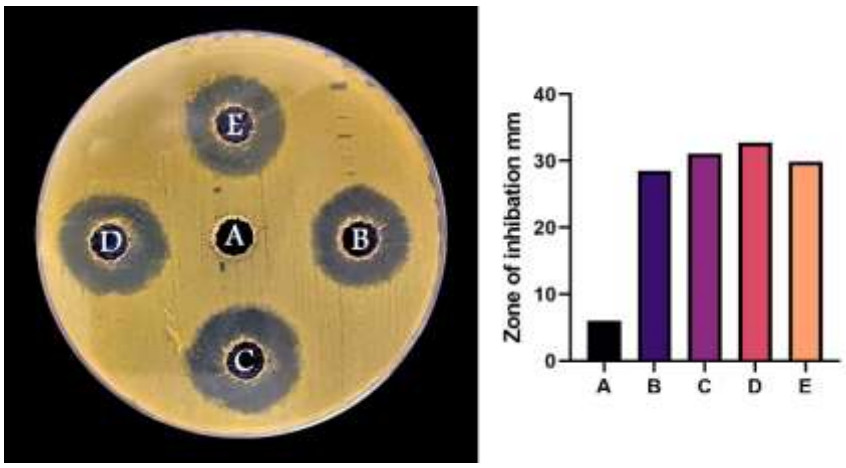

Figure 12. Antibacterial activity of (Sample B) against S. aureus. A, control. B, 25%. C, 50%. D, 75%. E, 100%.

4. CONCLUSION

Bi NPs were synthesized by PLAL using a 532 nm Nd:YAG laser at varied energies, number of pulses, and for various water temperatures. The presence of Bi NPs in the solution was verified via UV-Vis spectroscopy data yielding absorbance peaks at wavelengths lower than 270-280 nm. This result was further confirmed by EDXS analysis. The optimal conditions for water temperature (60˚C) and laser parameters (650 mJ, 410 pulses) were subsequently derived from UV-Vis spectrum data. These parameters were used as the sample preparation conditions to study the effects of water temperature on synthesized NPs. FESEM results indicated that NPs prepared at 60˚C had a smaller particle size and greater adsorption energy than Bi NPs prepared at 10˚C. Finally, antibacterial activity tests conducted with S. aureus bacteria exhibited larger inhibition zones than tests conducted with E. coli bacteria for Bi NPs prepared at 60 ˚C.

ACKNOWLEDGEMENTS

This research paper was partially supported by the Department of Laser and Optoelectronics Engineering, University of Technology, Iraq.

REFERENCES

[1] M. Hajipour , K. Fromm, A. Akbar Ashkarran, D. Jimenez de Aberasturi, I. Larramendi, T. Rojo, V. Serpooshan, W. Parak, M. Mahmoudi, Trends Biotechnol., vol. 30, issue. 10 (2012), pp. 499–511.

[2] V. Kohler, A. Vaishampayan, E. Grohmann, "Problematic Groups of Multidrug- Resistant Bacteria and Their Resistance Mechanisms" in Antibacterial Drug Discovery to Combat MDR, I. Ahmad, , S. Ahmad, Eds. Singapore: Springer Singapore (2019), pp. 25-69.

[3] S. Horikoshi, N. Serpone, "Introduction to Nanoparticles," in Microwaves Nanoparticle Synth. Fundam. Appl., S. Horikoshi, N. Serpone Eds. Wiley-VCH Verlag GmbH & Co. KGaA - Weinheim, Germany (2013), pp. 1–24.

[4] S. Shahzadi, N. Zafar, R. Sharif, "Antibacterial Activity of Metallic Nanoparticles," in Bacterial Pathogenesis and Antibacterial Control, Sahra, S. , Ed. London, United Kingdom, IntechOpen, (2018), pp. 51-71.

[5] E. O.Ogunsona, R.Muthuraj, E. Ojogbo, O.Valerio, T. H. Mekonnen, Appl. Mater. Today, vol. 18, issue October (2020), p. 100473.

[6] M. F.Altaee, L. A Yaaqoob., Z. K. Kamona, Iraqi J. Sci., vol. 61, issue 11 (2020), pp. 2888–2896.

[7] F. A. H.Mutlak, M. Jaber, H. Emad, Iraqi J. Sci., vol. 58, issue 4C (2017), pp. 2364–2369.

[8] H. Sallal, A. Abdul-Hameed, and F. Othman, Eng. Technol. J., vol. 38, issue 4A (2020), pp. 586–593.

[9] W. Pajerski, D. Ochonska, M. Brzychczy-Wloch, P. Indyka , M. Jarosz, M. Golda-Cepa, Z. Sojka, A. Kotarba, J. Nanoparticle Res., vol. 21, issue 8 (2019), p. 186.

[10] W. Zhang, B. Rittmann, Y. Chen, Environ. Sci. Technol., vol. 45, issue 6 (2011), pp. 2172–2178.

[11] G. Darabdharaa, P. Boruaha, N. Hussaina, P. Borthakura, B. Sharmaa, P. Senguptaa, M. Dasa, Colloids Surfaces A Physicochem. Eng. Asp., vol. 516 (2017), pp. 161–170.

[12] N. Burford, Y. Carpenter, E. Conrad, C. Saunders, "The Chemistry of Arsenic, Antimony and Bismuth", in Biological Chemistry of Arsenic, Antimony and Bismuth, H. Sun, Ed. John Wiley & Sons Ltd, (2010), pp 1-15.

[13] R. Wang, H. Li, and H. Sun, Elsevier, Encyclopedia of Environmental Health, 2nd ed., vol. 1, issue April (2019), pp. 415–423.

[14] V. Campos, A. Almaguer-Flores, D. Velasco-Aria, D. Díaz, S. Rodil, J. Mater. Sci. Eng. A, vol. 8, issue 4 (2018), pp. 142–146.

[15] R. Vazquez-Munoz, M. J. Arellano-Jimenez, J. L. Lopez-Ribot, BMC Biomed. Eng., vol. 2, issue 1 (2020), p. 11.
[16] C.-R. Claudio and S. Chellam, Nanomedicine, vol. 1, ch. 17 (2014) pp. 430–438.
[17] N. Baig, I. Kammakakam, W. Falath, Mater. Adv., vol. 2, issue 6 (2021), pp. 1821–1871.
[18] K. I. Hassoon, Eng. Technol. J., vol. 33, issue 2 (2015), pp. 338–345.
[19] K. Urabe, T. Kato, S. Stauss, S. Himeno, S. Kato, H. Muneoka, M. Baba,T. Suemoto, K. Terashima, J. Appl. Phys., vol. 114, issue 14 (2013), p. 143303.
[20] E. Fazio, B. Gökce, A. De Giacomo, M. Meneghetti, G. Compagnini, M. Tommasini, F. Waag, A. Lucotti, CG. Zanchi, PM. Ossi, M. Dell'Aglio, L. D'Urso, M. Condorelli, V. Scardaci, F. Biscaglia, L. Litti, M. Gobbo, G. Gallo, M. Santoro, S. Trusso, F. Neri, Nanomaterials, vol. 10, issue 11 (2020), p. 2317.
[21] D. Zhang, Z. Li, K. Sugioka, J. Phys. Photonics, vol. 3, issue 4 (2021), p. 042002.
[22] A. Addie, K. S. Khashaan, J. Saimon, A. Hassan, Iraqi J. Sci., vol. 62, issue 7 (2021), pp. 2197–2203.
[23] M. J. Haider, Eng. Technol. J., vol. 34, issue 7 (2016), pp. 1324–1334.
[24] L. Escobar-Alarcón et al., Adv. Mater. Res., vol. 976, issue July (2014) pp. 196–201.
[25] Y. Jun, Y. Zhu, Y. Wang, D. Ghim, X. Wu, D. Kim, H. Jung, Annu. Rev. Phys. Chem., vol. 73, issue 1 (2022)pp. 453-477.
[26] K.-J. Wu, E. C. M. Tse, C. Shang, Z. Guo, Prog. Mater. Sci., vol. 123, issue August (2022), p. 100821.
[27] V. Raghavan, "Phase Transformations" in Materials science and engineering: A First Course. Prentice-Hall of India Pvt.Ltd, (2011), pp. 201–237.
[28] N. T. K. Thanh, N. Maclean, S. Mahiddine, Chem. Rev., vol. 114, issue 15 (2014), pp. 7610–7630.
[29] A. Mohammed Fayaz, K. Balaji, P. T. Kalaichelvan, and R. Venkatesan, Colloids Surfaces B Biointerfaces, vol. 74, issue 1 (2009), pp. 123–126.
[30] M. M. H. Khalil, E. H. Ismail, K. Z. El-Baghdady, D. Mohamed, Arab. J. Chem., vol. 7 (2014), issue 6, pp. 1131–1139.
[31] H. Liu, H. Zhang, J. Wang, and J. Wei, Arab. J. Chem., vol. 13, issue 1 (2020), pp. 1011–1019.
[32] E. Solati, D. Dorranian, Bull. Mater. Sci., vol. 39, issue 7 (2016), pp. 1677–1684.
[33] H. Ammari, Y. Deng, and P. Millien, Arch. Ration. Mech. Anal., vol. 220, issue 1 (2016), pp. 109–153.
[34] N. Dinh, M. Leopold, R. Coppage, J. Inorg. Organomet. Polym. Mater., vol. 28, issue 6 (2018), pp. 2770–2778.
[35] Y.-R. Fang and X.-R. Tian, Chinese Phys. B, vol. 27, issue 6 (2018), p. 067302.
[36] S. A. Leslie and J. C. Mitchell, Palaeontology, vol. 50, issue. 6 (2007), pp. 1459–1461.
[37] P. Domenico, J. Reich, W. Madonia, and B. A. Cunha, J. Antimicrob. Chemother., vol. 38, issue 6, (1996), pp. 1031–1040.